



# Corrosion Behavior of Cold Sprayed Titanium Coatings and Free Standing Deposits

T. Hussain, D. G. McCartney, P. H. Shipway, and T. Marrocco

(Submitted May 5, 2010; in revised form July 20, 2010)

Cold gas dynamic spraying can be used to deposit oxygen-sensitive materials, such as titanium, without significant chemical degradation of the powder. The process is thus believed to have potential for the deposition of corrosion-resistant barrier coatings. However, to be effective, a barrier coating must not allow ingress of a corrosive liquid and hence must not have interconnected porosity. This study investigated the effects of porosity on the corrosion behavior of cold sprayed titanium coatings onto carbon steel and also of free standing deposits. For comparative purposes, a set of free standing deposits was also vacuum heat-treated to further decrease porosity levels below those in the as-sprayed condition. Microstructures were examined by optical and scanning electron microscopy. Mercury intrusion porosimetry (MIP) was used to characterize the interconnected porosity over a size range of micrometers to nanometers. Open circuit potential (OCP) measurements and potentiodynamic polarization scans in 3.5 wt.% NaCl were used to evaluate the corrosion performance. The MIP results showed that in cold sprayed deposits a significant proportion of the porosity was sub-micron and so could not be reliably measured by optical microscope based image analysis. In the case of free standing deposits, a reduction in interconnected porosity resulted in a lower corrosion current density, a lower passive current density, and an increase in OCP closer to that of bulk titanium. For the lowest porosity level, ~1.8% achieved following vacuum heat treatment, the passive current density was identical to that of bulk titanium. However, electrochemical measurements of the coatings showed significant substrate influence when the interconnected porosity of the coating was 11.3 vol.% but a decreased substrate influence with a porosity level of 5.9 vol.%. In the latter case, the OCP was still around 250 mV below that of bulk Ti. Salt spray tests confirmed these electrochemical findings and showed the formation of surface corrosion products following 24-h exposure.

**Keywords** cold spray, corrosion, heat treatment, porosity, titanium

## 1. Introduction

Titanium metal has excellent corrosion resistance in a number of aqueous media including salt water due to the presence of a tenacious oxide film (Ref 1) and so titanium

This article is an invited paper selected from presentations at the 2010 International Thermal Spray Conference and has been expanded from the original presentation. It is simultaneously published in *Thermal Spray: Global Solutions for Future Applications, Proceedings of the 2010 International Thermal Spray Conference*, Singapore, May 3-5, 2010, Basil R. Marple, Arvind Agarwal, Margaret M. Hyland, Yuk-Chiu Lau, Chang-Jiu Li, Rogerio S. Lima, and Ghislain Montavon, Ed., ASM International, Materials Park, OH, 2011.

T. Hussain, D.G. McCartney, and P.H. Shipway, Division of Materials, Mechanics and Structures, Faculty of Engineering, University of Nottingham, Nottingham, UK; and T. Marrocco, The Welding Institute (TWI) Ltd, Cambridge, UK. Contact e-mail: graham.mccartney@nottingham.ac.uk.

and its alloys have been used in a number of situations to protect steel structures and components from attack (Ref 2). However, deposition of protective coatings of titanium by thermal spraying processes is problematic due to the fact that titanium reacts readily with oxygen to form TiO<sub>2</sub> at elevated temperature. Hence the resultant coatings contain features such as oxide inclusions and interconnected pores which prevent the realization of the protective capabilities of titanium as a barrier coating. Indeed, a barrier coating needs to be entirely free from interconnected porosity to provide reliable corrosion protection. In the case of thermally sprayed coatings, a number of studies to evaluate corrosion behavior have been performed. For example, Zhao et al. (Ref 3) investigated the behavior of titanium which was arc sprayed in air and found that oxides and nitrides present in the coating degraded the corrosion resistance. Also a study by Ishikawa et al. (Ref 4) found that flame sprayed titanium coatings did not provide corrosion protection due to the high level of coating porosity. To avoid the problem of the reaction of titanium with the environment vacuum plasma and shrouded air plasma spraying have both been employed to deposit coatings (Ref 5, 6). However, a corrosion study of shrouded plasma sprayed titanium coatings in salt solution by Kinoshita et al. (Ref 6) using

potentiodynamic methods indicated that coating porosity significantly increased the corrosion rate compared to bulk titanium. More recently Kuroda and co-workers (Ref 7, 8) have reported the development of a modified high-velocity oxy-fuel (HVOF) process termed warm spraying which is reportedly capable of producing titanium coatings with porosity levels less than 1%. However, the corrosion rates of these warm sprayed coatings were also higher than bulk titanium because of the presence of interconnected porosity.

Evidently, there is a considerable interest in developing corrosion-resistant titanium coatings as barrier layers and so more recently much attention has focused on using the cold spray process to deposit titanium coatings. As an emerging technology, cold spray is being used increasingly to spray materials at high deposition rates in which significant particle melting is avoided (Ref 9-11). It has been found that metals such as copper can be deposited to produce coatings free from porosity as determined by open circuit potential (OCP) tests (Ref 12). Hence, there is now a growing interest in cold spray deposition of titanium with a significant body of work on titanium coatings and the effect of process parameters such as powder type, gas pressure, temperature, and type of gas on deposit characteristics including porosity (Ref 11, 13-19). A wide range of porosity values in cold sprayed titanium coatings has been reported in literature (24-0.5%), most of which was measured using image analysis techniques (Ref 11, 15-17, 19). The porosity of the coatings reported in the literature depends on the process parameters, type of process gas, and limitations of the spraying system. In general, higher in-flight particle velocity achieved from helium as a process gas resulted in denser titanium coatings (Ref 18). However, corrosion studies of cold sprayed titanium coatings are much less extensive. Wang et al. (Ref 2, 11) showed that the corrosion rate of coated steel substrates in salt solution was higher than bulk titanium due to interconnected porosity. However, there is no published data on the corrosion behavior of cold sprayed free standing titanium deposits to the knowledge of the authors. Furthermore, there is little attention given in the literature to quantifying the porosity of cold sprayed titanium by techniques other than image analysis of micrographs and in relating the porosity to corrosion behaviour in aqueous solutions.

Therefore, the aim of this study is to quantify and characterize the porosity of cold sprayed titanium deposits by mercury intrusion porosimetry (MIP), and to investigate the role of porosity in the corrosion behavior in salt water of both free standing titanium deposits and coatings on a steel substrate. Moreover, for comparative purposes, free standing deposits were heat-treated to reduce their porosity and the effect of this was also evaluated.

## 2. Experimental Methods

### 2.1 Materials

Commercially pure inert gas atomized titanium powder (LPW, Cheshire, UK) was used to produce the deposits.

The feedstock powder was spherical in shape with only a very small fraction exhibiting satellite particles (Fig. 1a). The particle size analysis measured by laser diffractometry (Malvern Mastersizer S, Malvern Instruments, Worcestershire, UK) showed that 90% of the particles were in the supplier specified size range of  $-30$  to  $+10$   $\mu\text{m}$  with approximately 10 vol.% below 10  $\mu\text{m}$  (Fig. 1b). The titanium powder was deposited onto carbon steel samples (0.037 wt.% C, 0.17 wt.% Mn, 0.01 wt.% P, 0.02 wt.% S, and balance Fe) of dimensions  $40 \times 25 \times 2$  mm.

### 2.2 Cold Gas Spraying of Titanium

The coatings and free standing deposits were prepared with a CGT<sup>TM</sup> Kinetiks<sup>®</sup> 4000/47 system at TWI Ltd. The de Laval nozzle had a length of 170 mm and a throat diameter of 2.7 mm with an area expansion ratio of  $\sim 6.5$ . The system utilized heated nitrogen gas both for the primary accelerating gas and the powder carrier gas. A high-pressure powder feeder (CGT) was used during the cold spraying process with a carrier gas flow rate of 3.7  $\text{m}^3/\text{h}$ , and powder feeder wheel speed of 3.5 rpm giving an approximate powder feed rate of 1.6 kg/h. The nozzle-substrate standoff distance for all the spray conditions was fixed at 40 mm.

The deposition conditions for the samples are presented in Table 1. The carbon steel substrates sprayed at 600 °C were grit blasted in a conventional manual grit blasting cabinet at 2.75 bar with a grit size of  $\sim 125$   $\mu\text{m}$ . It was not possible to produce a well-bonded coating onto a cabinet grit blasted carbon steel surface at the higher gas temperature. Hence, a more controlled grit blasting process using the cold spraying gun, which was mounted on a six axis robot, was used at 25 bar with a grit size of 45-90  $\mu\text{m}$ . The substrates were cleaned ultrasonically in a bath of acetone for 15 min, rinsed with methyl alcohol, and dried using compressed air immediately prior to spraying. Substrates were then clamped in a vice and the gun, mounted on the six axis robot manipulator scanned the surface of the samples at 600 mm/s. The increment of the scan was set at 0.75 mm. The deposits were built up using four passes of the gun.

A free standing deposit was obtained by carefully delaminating a coating from the steel substrate. The deposit sprayed at 600 °C gas temperature is referred to as free standing deposit FS1 and when coated onto carbon steel as C1. The deposit sprayed at 800 °C gas temperature is referred to as free standing deposit FS2, and when coated onto carbon steel as C2 in this article.

### 2.3 Postspray Heat Treatment

Free standing deposits were sealed in a quartz tube under a vacuum of  $10^{-4}$  Torr to avoid oxidation. The heat treatment was performed at 1050 °C for 60 min in a rapid heating furnace (Carbolite, Sheffield, UK) at a heating rate of 50 K/min. The heat treatment temperature was 150 K above the  $\beta$ -transus temperature of commercially pure titanium. Following heat treatment, the quartz tube was air cooled to room temperature.

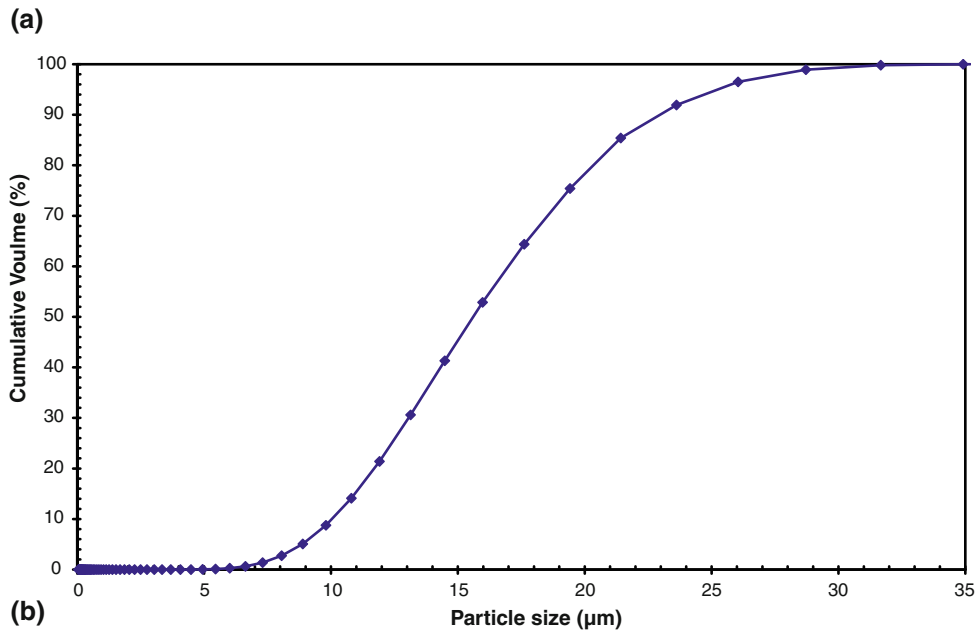
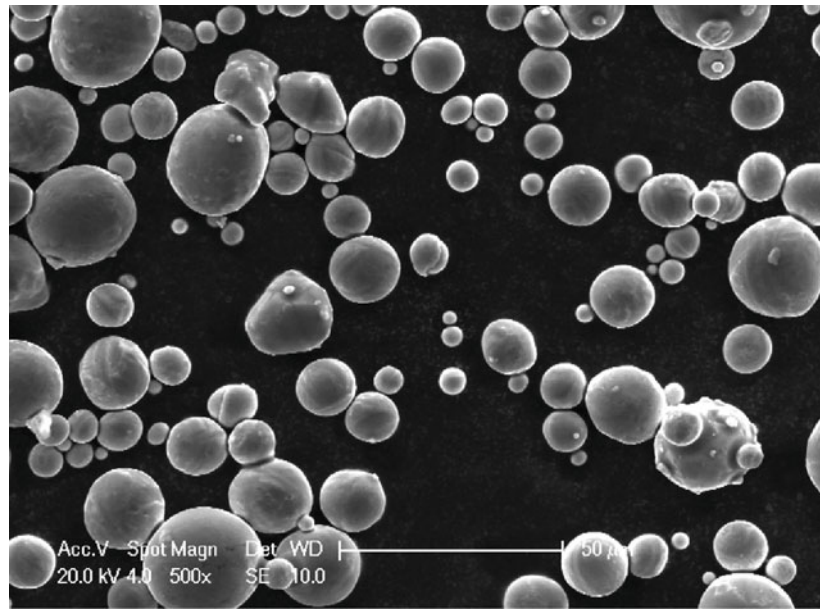


**Fig. 1** (a) SEM image of gas atomized titanium feedstock powder showing its near-spherical morphology. (b) Cumulative size distribution of titanium powder measured by laser diffractometry

**Table 1** Process parameters of cold spraying of titanium 600 and 800 °C coating

Spray parameters	Free standing deposit FS1/ coating C1 onto carbon steel	Free standing deposit FS2/ coating C2 onto carbon steel
Pressure, MPa	4	4
Primary gas temperature, °C	600	800
Primary gas flow rate, m <sup>3</sup> /h	86	80
Powder feed rate, g/min	27	27
Carrier gas flow rate, m <sup>3</sup> /h	3.7	3.7

## 2.4 Corrosion Tests

Potentiodynamic electrochemical tests of free standing titanium deposits and coatings were carried out using an ACM Gill 8 sequencer (ACM Instruments, Cumbria, UK) in a standard 3 electrode cell. A platinum metal strip of 100 mm<sup>2</sup> was used as an auxiliary electrode and the cell temperature was maintained at 30 ± 1 °C using a water bath. All the potentials were measured with respect to an Ag/AgCl secondary electrode. The samples were tested in a solution of 3.5 wt.% NaCl in de-ionized water and a flow of nitrogen gas was maintained at 0.1 L/min during the full

duration of the experiments. Nitrogen flowed through the solution for 30 min before the start of the test to stabilize the cell.

The substrate side of the free standing samples was lightly ground to remove any residual steel. The as-sprayed top surface of each sample was ground to P1200 grit finish to remove the top porous layer. The samples were painted with a stopping off lacquer to expose only 100 mm<sup>2</sup> for testing. Finally, the sample surfaces were degreased using methanol, cleaned with deionized water, and dried immediately before immersion.

The OCP of the specimens was measured during the first 60 min of immersion before starting the potentiodynamic scans. To conduct the polarization scans the samples were first lowered to a potential of 200 mV below the OCP and then scanned at a rate of 20 mV/min in the anodic direction. The scans were stopped when the potential of the samples reached an upper limit of 1800 mV above the rest potential,  $E_{\text{corr}}$ . The intersection of the anodic and cathodic linear extrapolations at the rest potential of potentiodynamic polarization scans (Tafel extrapolation) was taken as the corrosion current density,  $I_{\text{corr}}$ . The passive current density,  $I_{\text{pp}}$ , was taken as the current density of the passive region from the potentiodynamic polarization scans.

Reproducibility of the corrosion measurements was evaluated by running repeat tests on both free standing deposits and coatings. Three separate samples of free standing deposit FS1 and three samples of coating C2 were tested under the same conditions. The variations in measured values of the three free standing FS1 deposits were as follows: OCP  $\pm 30$  mV;  $E_{\text{corr}}$   $\pm 2.5$  mV;  $I_{\text{pp}}$   $\pm 0.005$  mA/cm<sup>2</sup>; and  $I_{\text{corr}}$   $\pm 0.0005$  mA/cm<sup>2</sup>. The variations in measured values of the three C2 coatings were as follows: OCP  $\pm 13$  mV;  $E_{\text{corr}}$   $\pm 30$  mV;  $I_{\text{pp}}$   $\pm 0.025$  mA/cm<sup>2</sup>; and  $I_{\text{corr}}$   $\pm 0.0005$  mA/cm<sup>2</sup>. These values are well within the typical range of experimental in electrochemical studies of this type. Therefore, graphs of typical OCP changes with time and potentiodynamic polarization scans for each sample are presented in this study.

Salt spray (fog) tests were performed for 24 h on coatings sprayed onto carbon steel with a dimension of 25 × 20 × 2.5 mm using a 5 wt.% NaCl solution. The back and the sides of the samples were covered with a red stopping off lacquer (toluene) to avoid any galvanic corrosion and only the top of the coating surface was exposed.

### 2.5 Sample Preparation and Characterization

Coating cross-sections were prepared by cutting with a diamond slitting wheel. The samples were sequentially ground using SiC paper and polished with 10:1 colloidal (0.1 μm) silica suspension and H<sub>2</sub>O<sub>2</sub> on a MD-Chem cloth (Struers, Rotherham, UK). Samples were examined by both optical and scanning electron microscopy. A FEI XL30 (FEI Europe, Eindhoven, The Netherlands) scanning electron microscope (SEM) operating at 20 kV was employed to examine the microstructure of the coatings using secondary electron (SE) imaging. The coatings were

lightly etched in Kroll's etchant (2% HF, 5% HNO<sub>3</sub>, and 95% H<sub>2</sub>O) for 15 s prior to examination in the microscope. The etching time needs to be kept constant as the etch attacks the microstructure and affects the visible features. The morphology of the powders and deposit top surfaces was also examined in the SEM using SE imaging.

The porosity of the free standing deposits was measured using a mercury intrusion porosimeter (Autopore IV, Micromeritics, Norcross, GA, USA). There are two ports in the porosimeter: a low- and a high-pressure ports. The low-pressure port evacuates any air trapped inside the sample and then fills it with mercury at 0.14 MPa. The sample is then transferred to the high-pressure port where the mercury infiltrates the sample at pressures up to 415 MPa. Free standing deposits of dimension 10 × 8 × 1 mm were used for the mercury intrusion tests. MIP can only be used to measure the open porosity which is connected to the surface of the deposits. Results are presented in the form of intrusion volume of mercury per gram of sample vs. pressure where pore diameter is then calculated from the pressure values using Washburn's equation.

$$D = -\left(\frac{1}{P}\right)4\gamma \cos \phi \quad (\text{Eq 1})$$

where  $D$  is the pore diameter,  $P$  is the applied pressure,  $\gamma$  is the surface tension of mercury, and  $\phi$  is the contact angle. Total mercury intrusion (mL/g) values were converted to volume percentages of porosity of the deposits assuming that the density of titanium is 4500 kg/m<sup>3</sup>.

## 3. Results

### 3.1 Microstructure and Corrosion Behavior of Free Standing Deposits

**3.1.1 Microstructure of Cold Sprayed Titanium.** The microstructure (unetched) of cold sprayed titanium sprayed at 600 °C (C1) and 800 °C (C2) process gas temperatures onto carbon steel is shown in Fig. 2(a) and (b). The microstructure of the coating C1 shows a porous top layer of 150 μm and a lower porosity bottom layer. The top porous layer is not as obvious in coating C2 which was sprayed at a higher process gas temperature. This porous top layer formation in cold sprayed titanium coating is similar to that reported previously by other researchers (Ref 13, 14). The coatings do not show cracking or any delamination along the coating-substrate interface, but do show the presence of fractured alumina (darker contrast) from the surface preparation methods. The thickness of coating C1 was 900 μm, whereas the thickness of coating C2 was 550 μm. This difference in coating thickness could be due to irregularities in powder feeding; although, the nominal powder feed rate and gun traverse speed in both cases were the same.

Figure 2(c) and (d) shows higher-magnification images of etched as-sprayed free standing deposits FS1 and FS2 taken from near the mid-plane of the coating. The

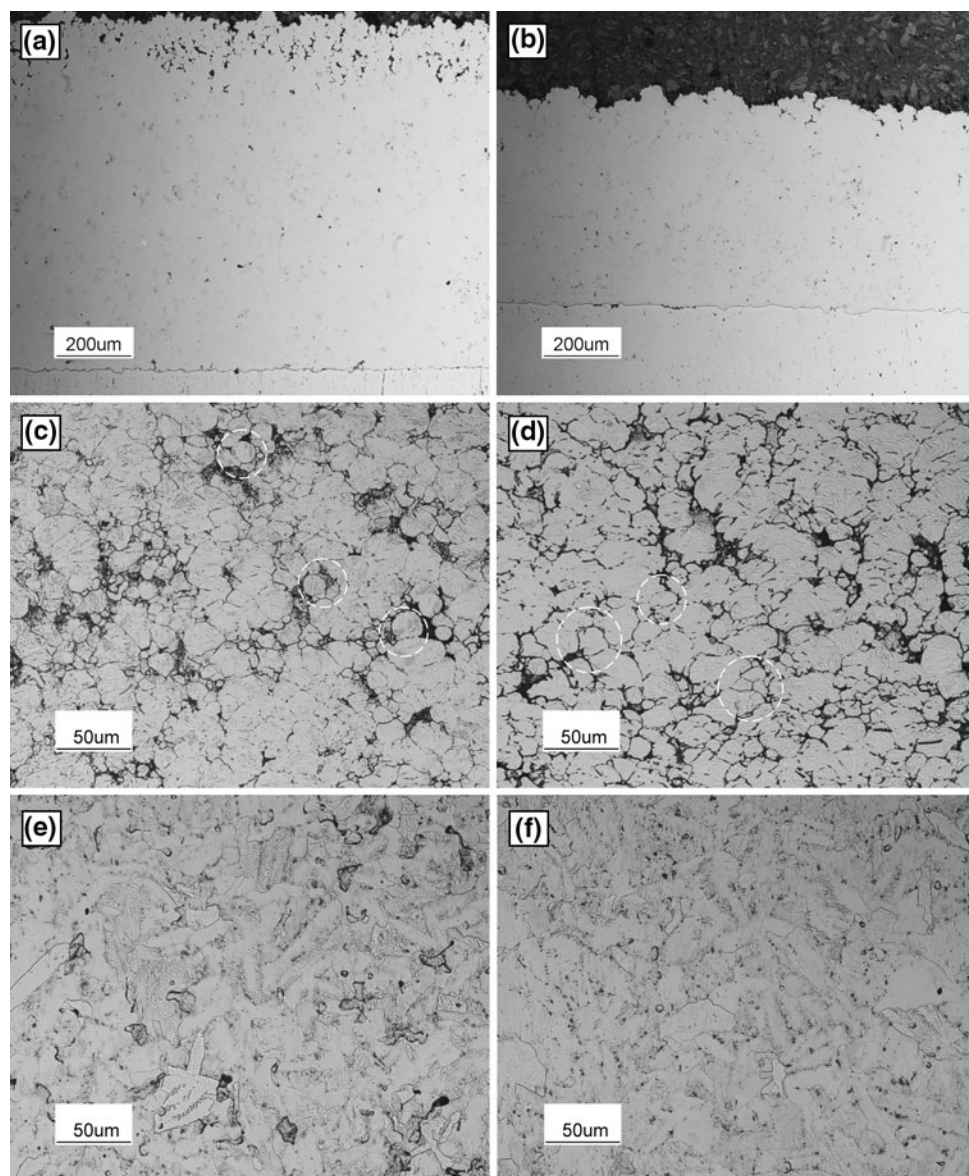


**Fig. 2** Lower-magnification unetched optical micrographs of titanium coatings onto carbon steel: (a) C1 and (b) C2. Higher-magnification etched optical micrographs of as-sprayed free standing deposits: (c) FS1 and (d) FS2. Higher-magnification etched optical micrographs of heat-treated free standing deposits: (e) FS1 and (f) FS2

microstructure is made up of a mixture of different sized particles, and voids are observed in both coatings at the interparticle boundaries. These voids are not visible in the unetched sample and result from loss of particles due to the attack of the particle boundaries by the etchant. In a number of places the initial spherical shape of the titanium powder particle was retained which indicates a lower degree of plastic deformation in FS1. These areas are marked with circles in Fig. 2(c). However, in Fig. 2(d) more extreme particle deformation is apparent (see circled regions). Because etching attacks the particle boundaries a prolonged etching results in losing particles from the deposits, so the “apparent” porosity depends on the duration of etching. Also in unetched samples

smearing of Ti during sample preparation can lead to an underestimate of porosity. Optical microscopy is thus an unreliable way of determining overall porosity in cold sprayed titanium coatings (Ref 20). This is why MIP was used to quantify the “actual” porosity in this study.

The free standing deposits, FS1 and FS2, after heat treatment at 1050 °C, are shown in Fig. 2(e) and (f) following etching. Most of the interparticle pores in FS2 deposit were eliminated following heat treatment due to recrystallization and grain growth at higher temperature, but a number of isolated regions of defects were still present in FS1. X-ray diffraction (XRD) analysis of both as-sprayed and heat-treated deposits showed the presence of only  $\alpha$ -Ti. No secondary phases were present within the

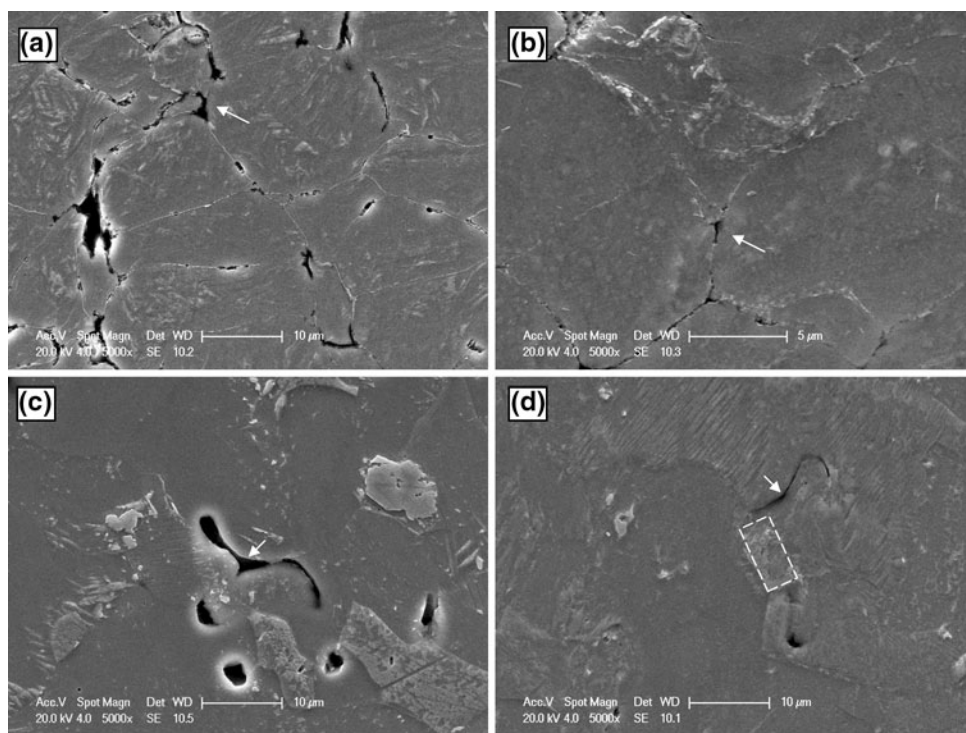


**Fig. 3** SEM images of etched samples showing changes in pore structure of free standing deposits before and after heat treatment. (a) As-sprayed FS1, (b) as-sprayed FS2, (c) heat-treated FS1, (d) heat-treated FS2 (arrows showing the interparticle pores and boxed region showing metallurgical bonding)

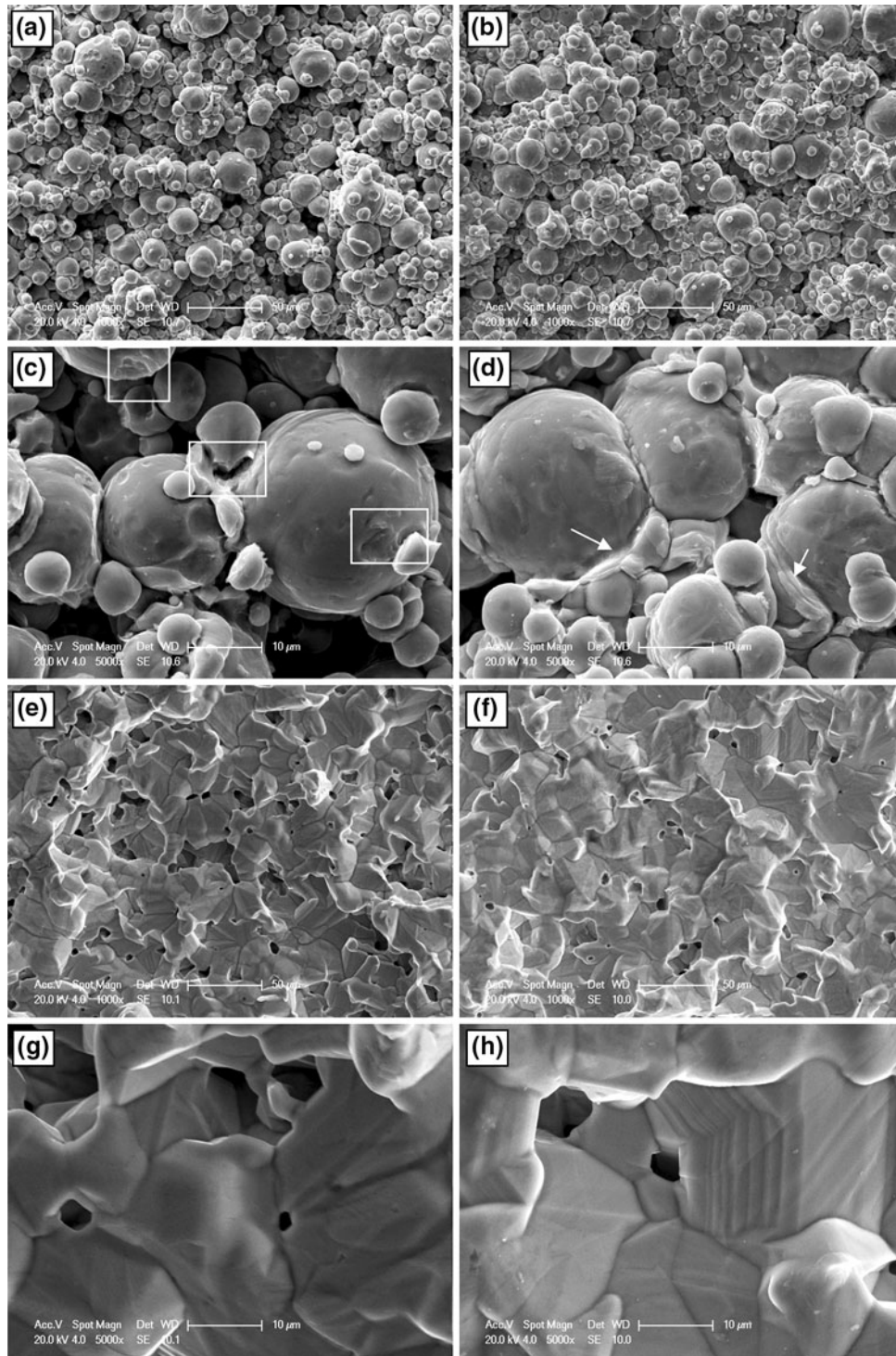
limits of XRD sensitivity (i.e., 1-2 vol.%). Figure 3 shows higher-magnification secondary electron (SE) images of the deposits before and after heat treatment. The pores in as-sprayed FS1 and FS2 deposits (Fig. 3a, b) are mostly at the interparticle boundaries and the gas atomized titanium powder particles show little evidence for pores within them. The heat-treated free standing FS1 deposit shows a reduction of interparticle voids and spheroidization of pores (Fig. 3c). Interparticle boundaries, nearly free from defects, were observed following heat treatment of FS2 and formation of metallurgical bonds at the interparticle splats (boxed region in Fig. 3d).

Figure 4(a) and (b) shows the as-sprayed top surface view of free standing deposits FS1 and FS2. The top surface of free standing deposit FS1 shows a higher surface roughness which corresponds to the top porous layer in the cross-sectional image in Fig. 2(a). Top surface of FS1 had a surface roughness ( $Ra$ ) value of 8  $\mu\text{m}$  and top surface of FS2 had a surface roughness ( $Ra$ ) value of 4  $\mu\text{m}$ . Figure 4(c) and (d) shows higher-magnification images of free standing deposits FS1 and FS2. FS1 deposit shows smaller titanium particles deposited onto larger titanium particles, and in some places, on larger particles, there is evidence of sliding and rebounding after impact. Rupture of the bonding of a titanium particle is also observed in the image, marked with boxes in the Fig. 4(c). In Fig. 4(d), the shear lips of titanium particles where the plastic flow of titanium occurred following the occurrence of adiabatic shear instability phenomena are marked with arrows (Ref

21). There is no evidence for re-bonding or ruptured bonding in this figure. Lower-magnification images of heat-treated top surfaces of free standing titanium deposits FS1 and FS2 are shown in Fig. 4(e) and (f). The heat-treated deposits show new grain growth and elimination of previous particle boundaries. Heat-treated free standing FS1 (Fig. 4e) shows larger intergrain voids when compared to heat-treated FS2 (Fig. 4f). Figure 4(g) and (h) shows higher-magnification images of heat-treated free standing deposits FS1 and FS2. In both the deposits, grain growth following heat treatment shows a reduction of pores with the formation of faceted grain boundaries.

**3.1.2 Porosity of Free Standing Deposits.** MIP was used to characterize the open pore size distribution of the FS1 and FS2 deposits, before and after heat treatment. Figure 5(a) shows the incremental mercury intrusion with respect to pore sizes of FS1 and FS2 deposits before and after heat treatment. The as-sprayed FS1 deposit has a pore size distribution of 0.3-8  $\mu\text{m}$ . Heat treatment of FS1 altered the pore size range to 0.6-2.5  $\mu\text{m}$ . The majority of the pores in the FS2 deposit were in the size range of 0.18-1.6  $\mu\text{m}$  with a smaller number of very fine pores of size 0.003-0.004  $\mu\text{m}$ . Heat treatment of FS2 showed a virtual complete elimination of larger pores and resulted in formation of very small pores of 0.006 to 0.013  $\mu\text{m}$ .

Figure 5(b) shows the cumulative intrusion of mercury per gram of sample vs. pore diameter. The cumulative intrusion for the as-sprayed FS1 deposit was 0.025 mL/g with a sharp increase of cumulative intrusion curve at



**Fig. 4** SEM images of the top view of free standing deposit before and after heat treatment. Lower-magnification images of as-sprayed (a) FS1 and (b) FS2. Higher-magnification images of (c) as-sprayed FS1 (*boxed area* showing rupture of bonds) and (d) as-sprayed FS2 (*arrows* showing viscous flow of material jet). Lower-magnification images of heat-treated free standing deposit showing changes in microstructure (e) heat-treated FS1 (f) heat-treated FS2. Higher-magnification images of heat-treated free standing deposits (g) heat-treated FS1 (h) heat-treated FS2

2-3  $\mu\text{m}$  pore sizes. The larger pores are filled up with mercury at lower pressure and smaller pores are infiltrated at higher pressure. Following heat treatment of FS1, the

total amount of intruded mercury decreased to 0.01 mL/g, i.e., decrease in the total pore volume. The cumulative intrusion of as-sprayed FS2 deposit was 0.013 mL/g, which

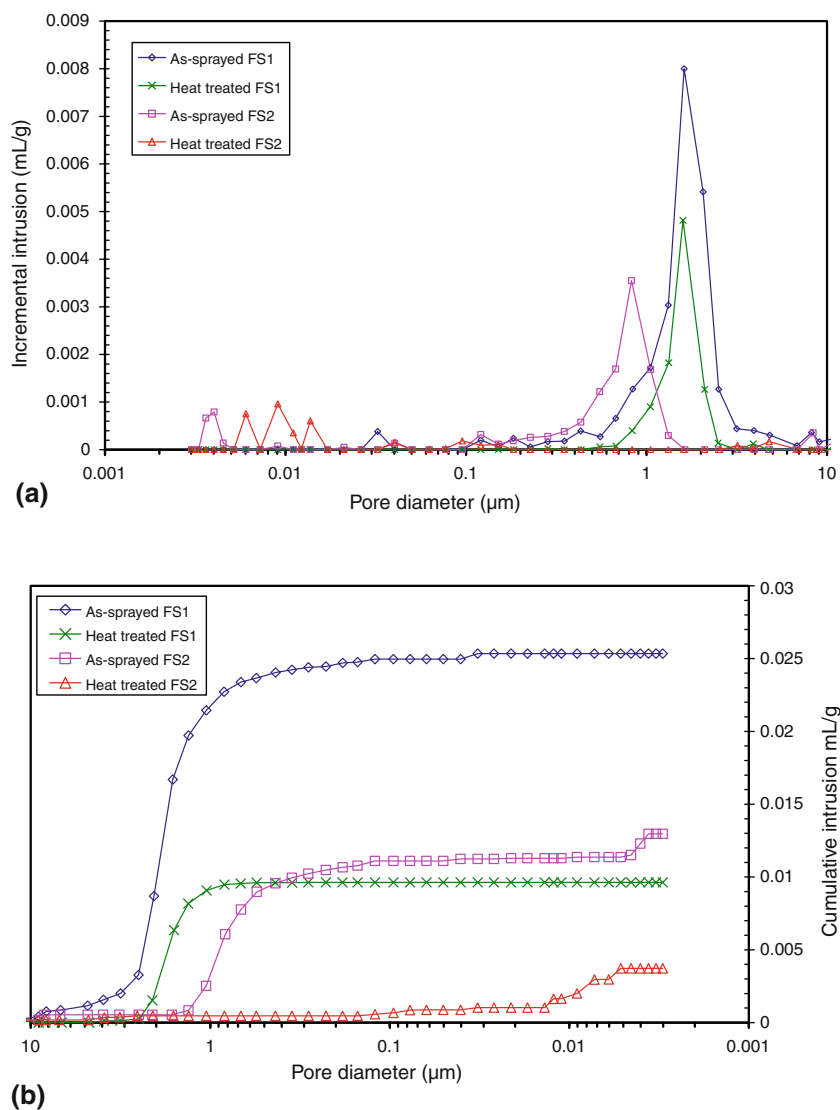


**Fig. 5** (a) Incremental intrusion of mercury vs. pore size of FS1 and FS2 deposits before and after heat treatment. (b) Cumulative mercury intrusion of the free standing FS1 and FS2 deposits before and after heat treatment

is half the amount when compared to as-sprayed FS1 deposit (0.025 mL/g). The slope of the FS2 cumulative intrusion curve sharply increases at the pore sizes of 1-2 μm. After heat treatment, FS2 deposit exhibited a cumulative intrusion of only 0.004 mL/g. The equivalent volume percentages of porosity from mercury intrusion tests are shown in Table 2. The last two columns of the table show the volume percentages of porosity of the deposits corresponding to pore sizes below and above 1 μm. In as-sprayed and heat-treated FS1, the pore sizes above 1 μm accounted for the majority of the porosity. However, in the as-sprayed and heat-treated FS2 deposit, the pores smaller than 1 μm accounted for the majority of the porosity. Evidently, optical microscopy can only detect pores of diameter approximately  $\geq 1$  μm and so will not detect these very fine pores.

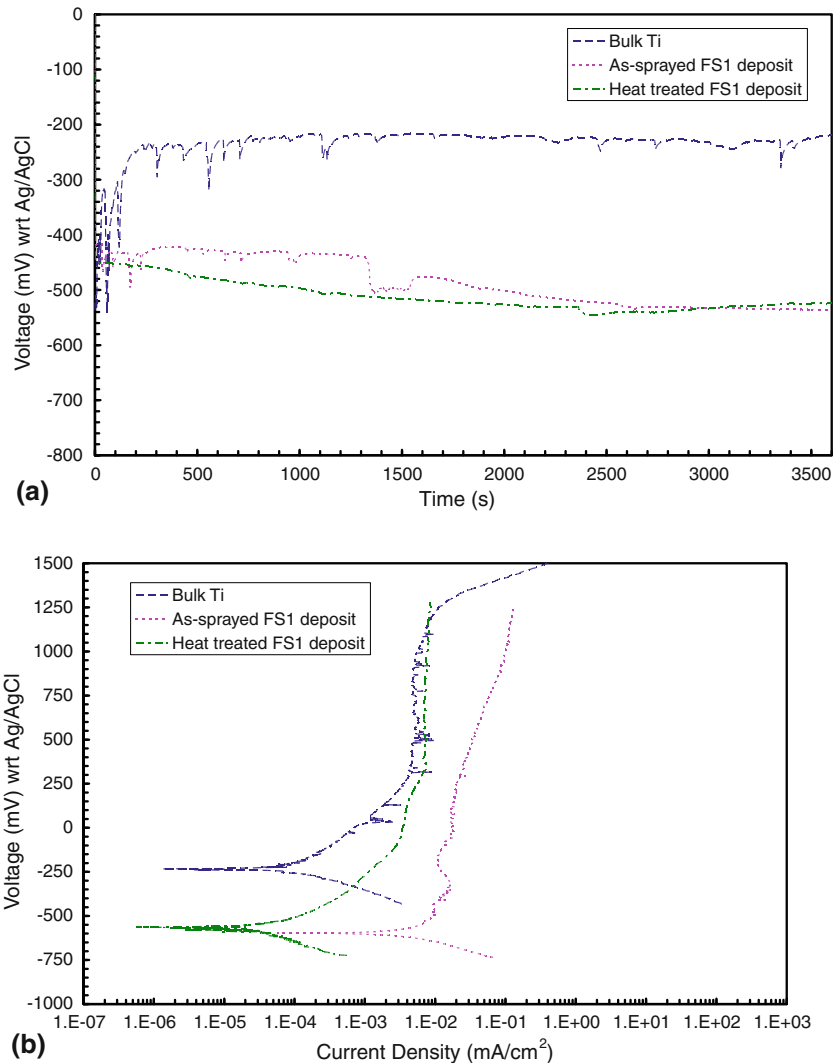
**3.1.3 Open Circuit Potential and Potentiodynamic Polarization of Free Standing Deposits.** Figure 6(a) shows the typical OCP measurements of bulk titanium, as-sprayed free standing deposit FS1, and heat-treated free standing deposit FS1 in 3.5% NaCl solution for 3600 s. The bulk titanium reached a steady state OCP of  $-220$  mV with respect to Ag/AgCl electrode within a few minutes of immersion. Both the OCPs of as-sprayed and heat-treated free standing FS1 deposits were  $\sim -530$  mV (Ag/AgCl).

Figure 6(b) shows typical potentiodynamic polarization scans of the bulk titanium, as-sprayed free standing deposit FS1, and heat-treated free standing FS1 deposit. The scan of bulk titanium showed typical active-passive behavior of a passivating metal. Bulk titanium had a passivation range of 250 to 1250 mV, after which it



**Table 2** Volume fraction of interconnected porosity of free standing FS1 and FS2 deposits before and after heat treatment

Process conditions	Total intrusion, mL/g	Total volume percentage of interconnected porosity, vol.%	Volume percentage of porosity with pore size >1 $\mu\text{m}$ , vol.%	Volume percentage of porosity with pore size <1 $\mu\text{m}$ , vol.%
As-sprayed FS1 deposit	0.025	11.3	9.9	1.4
Heat-treated FS1 deposit	0.010	4.5	4.0	0.5
As-sprayed FS2 deposit	0.013	5.9	1.4	4.5
Heat-treated FS2 deposit	0.004	1.8	0.2	1.6



**Fig. 6** (a) Open circuit potential (OCP) of bulk titanium, as-sprayed free standing FS1 deposit, and heat-treated free standing FS1 deposit in de-aerated 3.5 wt.% NaCl solution. (b) Potentiodynamic polarization scans of bulk titanium, as-sprayed free standing FS1 deposit, and heat-treated free standing FS1 deposit in the same solution

showed trans-passive behavior. The passive current density ( $I_{pp}$ ) of bulk titanium was  $0.005 \text{ mA/cm}^2$ . The as-sprayed free standing FS1 deposit showed “passive-like” behavior from 70 to 1250 mV, during which the current density increased from 0.017 to  $0.13 \text{ mA/cm}^2$ . It

also reached the limiting voltage value during the potentiodynamic polarization scan before the onset of trans-passive behavior. The heat treatment of free standing deposit FS1 resulted in a decrease of passive current density to  $0.007 \text{ mA/cm}^2$ . The  $E_{corr}$  of both the

**Table 3** Open circuit potential (OCP), rest potential ( $E_{\text{corr}}$ ), corrosion current density ( $I_{\text{corr}}$ ), and passive current density ( $I_{\text{pp}}$ ) of free standing deposits (FS1, FS2) before and after heat treatment, and coatings (C1, C2) onto carbon steel

Specimens	OCP after 1 h wrt Ag/AgCl, mV	$E_{\text{corr}}$ wrt Ag/AgCl, mV	Corrosion current density, $I_{\text{corr}}$ , mA/cm <sup>2</sup>	Passive current density, $I_{\text{pp}}$ , mA/cm <sup>2</sup>
Bulk titanium	-220	-233	$6.0 \times 10^{-5}$	0.005
As-sprayed FS1 deposit	-540	-565	$1.9 \times 10^{-3}$	0.017-0.13
Heat-treated FS1 deposit	-525	-600	$2.4 \times 10^{-5}$	0.007
As-sprayed FS2 deposit	-510	-483	$2.0 \times 10^{-4}$	0.005
Heat-treated FS2 deposit	-365	-373	$3.0 \times 10^{-5}$	0.005
Carbon steel	-750	-740	$3.0 \times 10^{-3}$	-
C1 coating onto carbon steel	-700	-836	$3.5 \times 10^{-3}$	1.1
C2 coating onto carbon steel	-500	-603	$2.0 \times 10^{-3}$	0.7

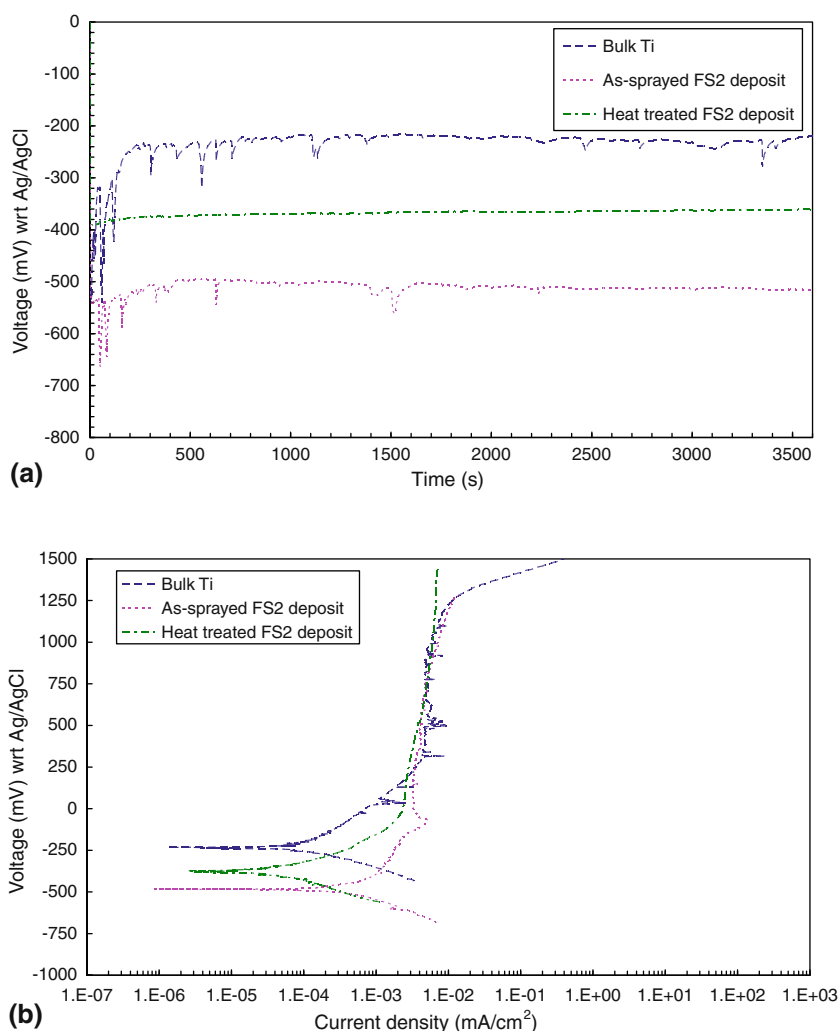


**Fig. 7** (a) Open circuit potential of bulk titanium, as-sprayed free standing FS2 deposit and heat-treated free standing FS2 deposit in de-aerated 3.5 wt.% NaCl solution. (b) Potentiodynamic polarization scans of bulk titanium, as-sprayed free standing FS2 deposit, and heat-treated free standing FS2 deposit in the same solution

as-sprayed deposit FS1 and the heat-treated deposit FS1 lies around  $\sim 580$  mV, but the  $I_{\text{corr}}$  value showed a decrease of two orders of magnitude after the heat treatment. The  $E_{\text{corr}}$  and  $I_{\text{corr}}$  values of all the samples are shown in Table 3.

OCP measurements of as-sprayed and heat-treated FS2 in 3.5 wt.% NaCl solution are shown in Fig. 7(a). The OCP of as-sprayed FS2 was  $-510$  mV and that of heat-treated FS2 was  $-365$  mV. The heat treatment of free standing deposit FS2 resulted in a shift of  $\sim 145$  mV in the

more positive direction, toward the bulk titanium. This is a significant difference from the behavior of heat-treated FS1.

Figure 7(b) shows the potentiodynamic polarization of as-sprayed and heat-treated FS2 deposit. These showed similar passive current density ( $0.005 \text{ mA/cm}^2$ ) to bulk titanium. The  $E_{\text{corr}}$  values of the as-sprayed and the heat-treated FS2 deposits showed similar trends to OCP measurements. The  $I_{\text{corr}}$  value of the heat-treated FS2 deposit reduced to  $3 \times 10^{-5}$  from  $2 \times 10^{-4} \text{ mA/cm}^2$  following heat treatment.

### 3.2 Corrosion Behavior of Coatings onto Carbon Steel

Figure 8(a) shows the OCP of as-sprayed C1 (porosity ~11 vol.%) and C2 (porosity ~6 vol.%) coatings onto carbon steel, bulk titanium, and bulk carbon steel for

3600 s. OCP of bulk titanium was  $-220 \text{ mV}$  and carbon steel reached a steady OCP of  $-750 \text{ mV}$  after 1200 s of immersion. As-sprayed C1 coating onto carbon steel reached a steady state OCP of  $-700 \text{ mV}$  after 200 s of immersion and remained at that level during the full length of the experiment. As-sprayed C2 coating onto carbon steel showed a decreasing trend in OCP measurements, which started at  $-320 \text{ mV}$  upon immersion and gradually dropped to  $-500 \text{ mV}$  after 3600 s.

Potentiodynamic polarization scans of C1 and C2 coatings onto carbon steel, bulk titanium, and carbon steel are shown in Fig. 8(b). C1 coating showed an  $I_{\text{corr}}$  value of  $3.5 \times 10^{-3} \text{ mA/cm}^2$  and  $E_{\text{corr}}$  value of  $-836 \text{ mV}$ ; and C2 coating showed an  $I_{\text{corr}}$  value of  $2 \times 10^{-3} \text{ mA/cm}^2$  and  $E_{\text{corr}}$  value of  $-603 \text{ mV}$  (Table 3). C1 coating onto carbon steel showed “passive-like” corrosion current density of  $1.1 \text{ mA/cm}^2$ , and C2 coating onto carbon steel showed a value of  $0.7 \text{ mA/cm}^2$ ; these are around two orders of

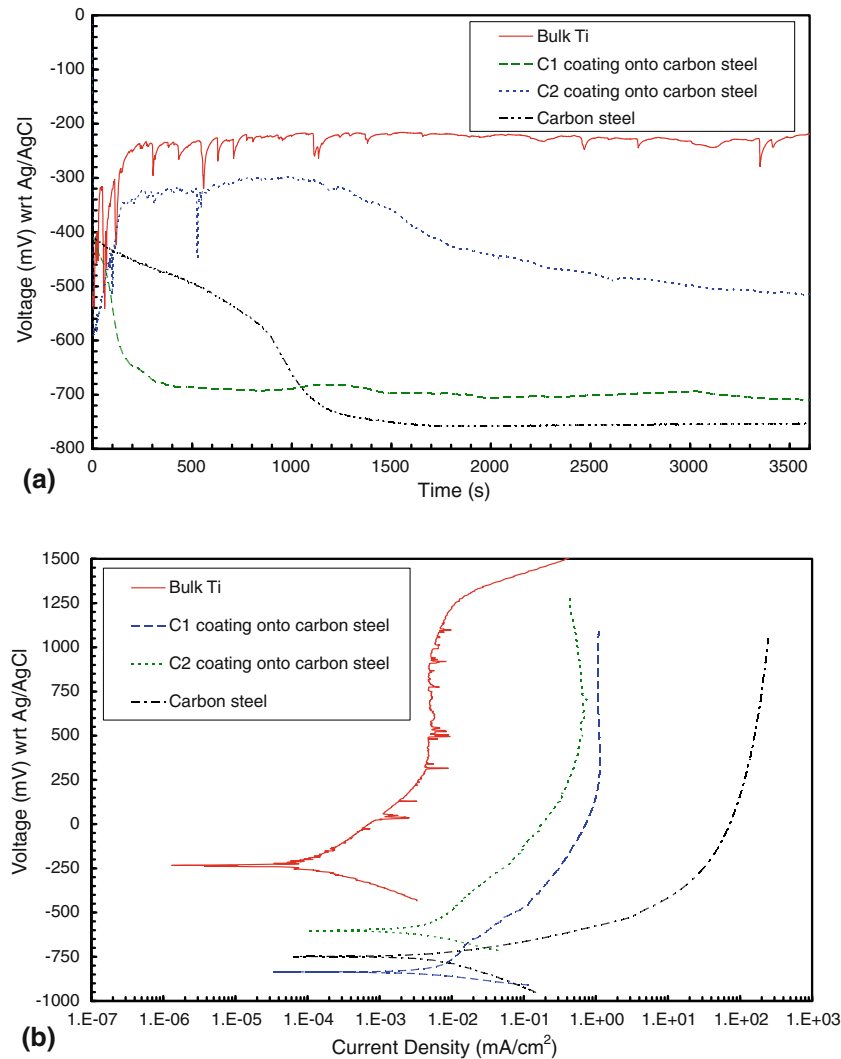


**Fig. 8** (a) Open circuit potential of bulk titanium, carbon steel, C1 coating onto carbon steel, and C2 coating onto carbon steel in de-aerated 3.5 wt.% NaCl solution. (b) Potentiodynamic polarization scans of bulk titanium, carbon steel, C1 coating onto carbon steel, and C2 coating onto carbon steel in the same solution

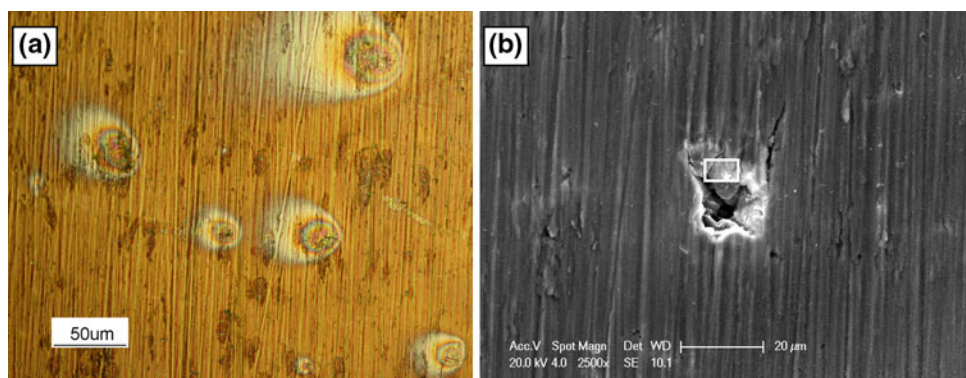


**Fig. 9** (a) Optical microscope image of the top view of C1 coating onto carbon steel showing localized corrosion following open circuit potential and potentiodynamic polarization scans in 3.5 wt.% NaCl. (b) Higher-magnification SEM (SE) image of one of those areas attacked by the corrosive solution

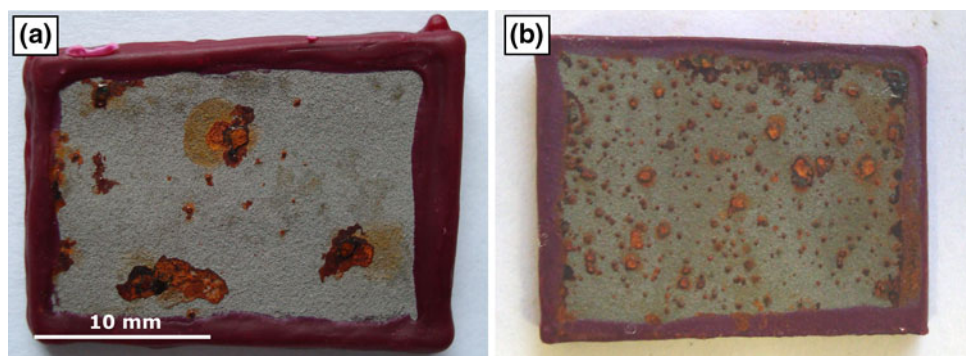


**Fig. 10** Low-magnification optical macrographs of salt spray (fog) sample surface after 24 h of exposure. (a) C1 coating onto carbon steel showing larger localized corrosion spots and (b) C2 coating onto carbon steel showing more uniformly distributed corrosion spots

magnitude greater than bulk titanium passive current density of  $0.005 \text{ mA/cm}^2$ . A piece of carbon steel substrate was also tested under similar conditions for reference. Carbon steel had an  $I_{\text{corr}}$  value of  $3 \times 10^{-3} \text{ mA/cm}^2$  and  $E_{\text{corr}}$  value of  $-750 \text{ mV}$ . The current density of carbon steel increased rapidly with overpotential and reached a limiting value of  $1000 \text{ mA/cm}^2$  at  $1050 \text{ mV}$ .

Figure 9(a) and (b) shows the top surface of C1 coating after potentiodynamic polarization at low and high magnifications. The optical microscope image of Fig. 9(a) shows evidence of localized corrosion on the sample surface, where the electrolyte percolated through the coating and attacked the carbon steel substrate. Figure 9(b) shows a higher-magnification SEM image of one of the localized corrosion regions. Energy dispersive x-ray analysis in the SEM of the boxed region showed the presence of iron, oxygen, sodium, and chlorine on the titanium coating surface.

Figure 10(a) and (b) shows the salt spray (fog) test results of C1 and C2 coatings onto carbon steel after 24 h of exposure. C1 coating showed severely attacked pits on the surface, where distinctive yellow rust from the corrosion of carbon steel substrate was present. The surface of

C2 coating showed a large number of small corrosion spots after the test. The coating C2 shows uniformly distributed corrosion product over the entire surface as opposed to a few large corrosion pits in the C1 coating.

## 4. Discussion

### 4.1 Microstructure and Porosity of Titanium

Although it is possible to produce a pore-free microstructure using cold spray from ductile face centered cubic copper (Ref 22), it is more difficult to produce a pore-free deposit from titanium. Titanium may be more difficult to densify in cold spraying due to its hexagonal closed pack (hcp) crystal structure and its lower density (Ref 16, 23). A less deformed top porous layer is clearly observed in the deposits sprayed at  $600^\circ\text{C}$ , whereas, this porous layer is less evident in the deposits sprayed at  $800^\circ\text{C}$ . It can be argued that there are two effects taking place at the higher process gas temperature. First, the particles reach a higher in-flight velocity due to a higher Mach number inside the gun and secondly, the particles reach a higher temperature

in the gas stream. According to the energy balance theory the initial kinetic energy of a particle before impact is the sum of the energy dissipated as plastic deformation plus recoverable strain energy (Ref 24). A higher particle velocity results in a greater kinetic energy which enhances plastic deformation. Also heating of the particles changes the initial state of impacting bodies due to thermal softening that results in a decrease of flow stress. Also, the porosity of titanium deposits decreases with increasing the distance from the coating top surface because the particles at the bottom of the coating experience more of a peening effect than the particles deposited at the top surface (Ref 13).

The shear lips of the titanium particles observed at the top surface of the coating sprayed at 800 °C process gas temperature (Fig. 4d) can be attributed to the highly localized temperature increase at the impacting interface due to a relatively low thermal conductivity and a low diffusivity of titanium (Ref 15). During this high strain rate plastic deformation of titanium, much of the work done is converted to heat (Ref 25). On the other hand, partial bonding and ruptured bonds in the deposits sprayed at 600 °C (Fig. 4c) can be attributed to elastic relief on unloading during the impact phenomena (Ref 26). These differences in deformation of the particles and thermal softening resulted in an open porosity of ~6 vol.% in the deposits sprayed at 800 °C when compared to ~11 vol.% of the deposits sprayed at 600 °C as determined from MIP.

It was evidenced from the micrographs, Fig. 4(g) and (h), that the heat treatment of free standing titanium deposits above the  $\beta$ -transus temperature resulted in grain growth and reduction in porosity. Titanium has an adherent oxide ( $\text{TiO}_2$ ) layer which has to be disrupted to form metallurgical bonds (Ref 20, 27). Moreover, the oxide layer on the metal surface acts as a diffusion barrier for many metals, but  $\text{TiO}_2$  does not hinder the formation of metallurgical bonds during heat treatment because both  $\alpha$  and  $\beta$  phases of titanium are known to dissolve oxygen interstitially (Ref 28). Therefore, during vacuum heat treatment new grains were formed and grain growth took place, which eliminated the sprayed particle boundaries (Ref 29). Consequently, the interparticle pores in the as-sprayed deposits were pinned down at the new grain boundaries. In summary, heat treatment resulted in a reduction of open porosity in FS1 from ~11 to ~5 vol.% and in FS2 from ~6 to ~2 vol.%.

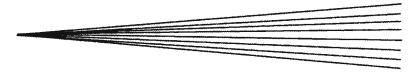
MIP measured the interconnected porosity of the as-sprayed and the heat-treated free standing deposits down to a few nanometers of pore sizes, estimated from Eq 1. This is well below the resolution of an optical microscope. If an optical microscope with a typical resolution of 1  $\mu\text{m}$  were to be used to measure the porosity of heat-treated FS2, the deposit would appear to have a porosity of only ~0.2% because the sub-micron pores would not be resolved (Table 2). However, the majority of the pores in the heat-treated FS2 were of sub-micron sizes which account for a porosity of 1.6 vol.%. Moreover, MIP has a unique advantage in measuring the volume percentage of porosity in cold sprayed coatings when compared with

thermally sprayed metals because the formation of oxide can be neglected. Therefore MIP cumulative intrusion values can readily be converted to volume percentage of porosity using the known density of metallic Ti. In thermally sprayed coatings, the volume percentage and density of any oxide inclusions also need to be known before the cumulative intrusion values in milliliter of mercury per gram of sample can be converted to volume percentage of porosity.

#### 4.2 Corrosion Behavior of Free Standing Deposits

In thermally sprayed coatings, OCP measurements and potentiodynamic polarization scans have been widely used to evaluate the corrosion behavior (Ref 30-33). In the present potentiodynamic experiments, heat-treated FS1, as-sprayed FS2, and heat-treated FS2 deposits show a passive current density similar to the bulk titanium, which means that the change in porosity level from ~6 to ~2 vol.% does not have a significant effect on the passive current density. However, the as-sprayed free standing deposit FS1 with a porosity of ~11 vol.% shows an increased passive current density (by 1-2 orders of magnitude). This could be due to an increase in “true surface area” taking part in the corrosion reactions. In support of this, a similar increase in passive current density with increasing porosity in sintered and warm sprayed titanium has also been reported in literature (Ref 7, 34). Moreover, in contrast to APS, arc, or flame sprayed titanium deposits, cold sprayed titanium deposits are apparently free from oxides and nitrides, and hence the increase in passive current density is unlikely to arise from the presence of such phases. In this study, the OCPs of all the deposits show more negative values when compared to the bulk titanium, which means that the deposits had active surfaces and higher thermodynamic tendency to corrosion (Ref 3). Also, the OCPs of the deposits did not show any decreasing trend with time because of the stability of the protective oxide film (Ref 35). Also it would appear that OCPs and  $E_{\text{corr}}$  values are more sensitive to small amounts of porosity than are passive current densities. In Fig. 7(a), the heat-treated deposit FS2 is seen to be cathodic with respect to bulk titanium, whereas Fig. 7(b) shows an identical passive current density.

Corrosion current density ( $I_{\text{corr}}$ ) is directly proportional to the corrosion rate of the material and in this study, potentiodynamic polarization scans showed that  $I_{\text{corr}}$  of free standing deposit FS2 (~6 vol.% porosity) is an order of magnitude smaller than FS1 (~11 vol.%). In addition, heat treatment of both FS1 and FS2 deposits reduced the  $I_{\text{corr}}$  by 1-2 orders of magnitude. It was reported in several studies that corrosion performance of sprayed deposits improved following heat treatment (Ref 31, 36). Heat treatment of porous titanium deposits eliminates the smaller pores to produce a more homogenous structure and the surface oxide of the particles is removed during heat treatment in a vacuum (Ref 36). Moreover, cold sprayed deposits contain highly deformed particles because of the high-velocity impacts and high strain rate plastic deformation of the particles (Ref 37). These highly



deformed particles could act as preferential sites for corrosion (Ref 9). Heat treatment of the as-sprayed deposits also eliminates these high stressed regions and thus reduces the preferential corrosion attack.

### 4.3 Corrosion Behavior of Coatings onto Carbon Steel

OCP is widely used as a method to assess the effect of interconnected porosity in sprayed coatings (Ref 2, 10, 33). A barrier coating layer will show an OCP very close to that of the coating material, whereas a porous coating, which allows the corrosive liquid to attack the substrate, will show an OCP closer to the substrate material. In this study, both the coated samples C1 and C2 had OCP values in between bulk titanium and carbon steel substrate, which indicates salt solution percolation through the coatings. As-sprayed C2 coating (porosity ~6 vol.%) had an OCP closer to bulk titanium for first few hundred seconds and then the OCP decreased; presumably when the solution started percolating through the coating and attacking the substrate. However, with C1 coating (porosity ~11 vol.%) the OCP decreased to the carbon steel value within few tens seconds of immersion. Furthermore, C1 coating had a coarser pore size distribution (0.3-8  $\mu\text{m}$ ) than that of C2 (0.18-1.6) which possibly allowed the solution to percolate through the coating readily. It should also be mentioned that although C1 coating was thicker than C2 coating, by around ~300  $\mu\text{m}$ , this increased thickness did not provide any increased corrosion resistance! Clearly, therefore, less interconnected porosity in coatings plays the major role in corrosion resistance over increased thickness.

Salt spray test results also confirmed the lack of barrier-like properties of coatings C1 and C2 (Fig. 10a, b). It is clear that C1 coating, which had a higher porosity and larger pores, exhibited only a few but large corrosion spots when compared to C2 coating. One explanation for this is that once the corrosion of the substrate started due to galvanic effect, it had a higher driving force to continue corroding at the attacked sites instead of forming new pits. In aggressive environments like salt spray test, micro galvanic cells are formed across the titanium-carbon steel interface which ultimately results in delamination of the coating.

As expected, potentiodynamic polarization scans of the coatings onto carbon steel resulted in a higher anodic corrosion current when compared to the bulk titanium sheet. These differences in current density were also due to the percolation of the solution through the coating. The lower amount of porosity in C2 coating when compared to C1 resulted in a decrease in anodic current. A study by Wang et al. (Ref 11) also showed that cold sprayed titanium coating with a lower porosity resulted in a lower anodic corrosion current in salt solution. However, the densest coating (1.6%), in that study, which was measured using image analysis techniques, showed increased anodic corrosion current (by two orders of magnitude) when compared to bulk titanium. Moreover, this behavior of

reduction of anodic current with decreasing porosity was also observed in HVOF coatings and plasma sprayed titanium coatings because of a reduction in active corrosion sites on the substrate (Ref 36, 38).

Future work to improve the corrosion performance of cold sprayed titanium coating should thus focus on enhancing the particle deformation during cold spraying to ensure the elimination of even sub-micron porosity which cannot be observed in the optical microscope but is measurable using MIP. Surface treatment of the top layer of titanium coatings could also be investigated to achieve barrier coating properties.

## 5. Conclusions

Titanium was deposited by cold gas dynamic spraying using two different process parameters designed to reduce porosity. The porosity of the deposits was characterized by MIP. The deposits were heat-treated to reduce porosity and the effect of porosity on the corrosion performance of free standing titanium deposits was studied in 3.5 wt.% NaCl solution. Corrosion performance of titanium coatings onto carbon steel was also investigated in the same solution using electrochemical methods and salt spray tests. The following conclusions were drawn from the above study:

- Cold spraying using  $\text{N}_2$  as a process gas heated to 800 °C can deposit titanium with less interconnected porosity than  $\text{N}_2$  gas at 600 °C due to a higher degree of particle deformation on impact. MIP can be successfully used to measure total interconnected porosity, including sub-micron pores, in free standing deposits.
- A pore free microstructure of titanium deposit could not be achieved from cold spraying alone. However, vacuum heat treatment of free standing titanium deposits significantly reduced the interconnected porosity. Pores above 1  $\mu\text{m}$  were reduced to 0.2 vol.% and the total interconnected porosity to 1.8 vol.% following heat treatment of deposits produced at a process gas temperature of 800 °C.
- OCPs and rest potentials ( $E_{\text{corr}}$ ) are more sensitive to small amounts of porosity than are passive current densities ( $I_{\text{pp}}$ ). However, OCP values of free standing titanium deposits were, in all cases, lower than that of bulk titanium due to porosity even after vacuum heat treatment.
- Electrochemical corrosion studies of the titanium coatings on carbon steel substrate showed significant substrate influence at the levels of porosity arising from deposition at both 600 and 800 °C. OCPs and passive current densities of the coatings were significantly different from that of bulk titanium due to the interconnected porosity. Salt spray tests also confirmed the presence of interconnected porosity in these coatings.

## Acknowledgments

T. Hussain acknowledges financial support from the University of Nottingham through the award of an Overseas Research Studentship (ORS) and industrial sponsorship from TWI Ltd., UK for his research. The authors thank Dr. C M Lee from TWI, Cambridge, UK for useful discussion on the corrosion measurement.

## References

- J.F. Sun, Y. Han, and K. Cui, Innovative Fabrication of Porous Titanium Coating on Titanium by Cold Spraying and Vacuum Sintering, *Mater. Lett.*, 2008, **62**(21-22), p 3623-3625
- H.R. Wang, W.Y. Li, L. Ma, J. Wang, and Q. Wang, Corrosion Behavior of Cold Sprayed Titanium Protective Coating on 1cr13 Substrate in Seawater, *Surf. Coat. Technol.*, 2007, **201**(9-11), p 5203-5206
- W.M. Zhao, C. Liu, L.X. Dong, and Y. Wang, Effects of Arc Spray Process Parameters on Corrosion Resistance of Ti Coatings, *J. Therm. Spray Technol.*, 2009, **18**(4), p 702-707
- K. Ishikawa, T. Suzuki, Y. Kitamura, and S. Tobe, Corrosion Resistance of Thermal Sprayed Titanium Coatings in Chloride Solution, *J. Therm. Spray Technol.*, 1999, **8**(2), p 273-278
- T. Kinoshita, S. Chen, P. Siitonen, and P. Kettunen, Densification of Plasma-Sprayed Titanium and Tantalum Coatings, *J. Therm. Spray Technol.*, 1996, **5**(4), p 439-444
- T. Kinoshita, S.L. Chen, P. Siitonen, and P. Kettunen, Corrosion Properties of Shrouded Plasma Sprayed Titanium Coatings, *Thermal Spraying: Current Status and Future Trends*, A. Ohmori, Ed., May 22-26, 1995 (Kobe, Japan), High Temperature Society of Japan, 1995, p 573-576
- J. Kawakita, H. Katanoda, M. Watanabe, K. Yokoyama, and S. Kuroda, Warm Spraying: An Improved Spray Process to Deposit Novel Coatings, *Surf. Coat. Technol.*, 2008, **202**(18), p 4369-4373
- J. Kawakita, S. Kuroda, T. Fukushima, H. Katanoda, K. Matsuo, and H. Fukunuma, Dense Titanium Coatings by Modified HVOF Spraying, *Surf. Coat. Technol.*, 2006, **201**(3-4), p 1250-1255
- K. Balani, T. Laha, A. Agarwal, J. Karthikeyan, and N. Munroe, Effect of Carrier Gases on Microstructural and Electrochemical Behavior of Cold-Sprayed 1100 Aluminum Coating, *Surf. Coat. Technol.*, 2005, **195**(2-3), p 272-279
- H. Koivuluoto, J. Näkki, and P. Vuoristo, Corrosion Properties of Cold-Sprayed Tantalum Coatings, *J. Therm. Spray Technol.*, 2009, **18**(1), p 75-82
- H.R. Wang, B.R. Hou, J. Wang, Q. Wang, and W.Y. Li, Effect of Process Conditions on Microstructure and Corrosion Resistance of Cold-Sprayed Ti Coatings, *J. Therm. Spray Technol.*, 2008, **17**(5), p 736-741
- H. Koivuluoto, M. Honkanen, and P. Vuoristo, Cold-Sprayed Copper and Tantalum Coatings—Detailed FESEM and TEM Analysis, *Surf. Coat. Technol.*, 2010, **204**(15), p 2353-2361
- C.J. Li and W.Y. Li, Microstructure Evolution of Cold-Sprayed Coating During Deposition and through Post-Spraying Heat Treatment, *Trans. Nonferrous Met. Soc. China (English Edn)*, 2004, **14**(Suppl. 2), p 49-54
- C.J. Li and W.Y. Li, Deposition Characteristics of Titanium Coating in Cold Spraying, *Surf. Coat. Technol.*, 2003, **167**(2-3), p 278-283
- W.Y. Li, C. Zhang, H.T. Wang, X.P. Guo, H.L. Liao, C.J. Li, and C. Coddet, Significant Influences of Metal Reactivity and Oxide Films at Particle Surfaces on Coating Microstructure in Cold Spraying, *Appl. Surf. Sci.*, 2007, **253**(7), p 3557-3562
- T. Marrocco, D.G. McCartney, P.H. Shipway, and A.J. Sturgeon, Production of Titanium Deposits by Cold-Gas Dynamic Spray: Numerical Modeling and Experimental Characterization, *J. Therm. Spray Technol.*, 2006, **15**(2), p 263-272
- S.H. Zahiri, C.L. Antonio, and M. Jahedi, Elimination of Porosity in Directly Fabricated Titanium Via Cold Gas Dynamic Spraying, *J. Mater. Process. Technol.*, 2009, **209**(2), p 922-929
- S.H. Zahiri, W. Yang, and M. Jahedi, Characterization of Cold Spray Titanium Supersonic Jet, *J. Therm. Spray Technol.*, 2009, **18**(1), p 110-117
- W. Wong, A. Rezaeiann, E. Irissou, J.G. Legoux, and S. Yue, Cold Spray Characteristics of Commercially Pure Ti and Ti-6Al-4v, *Adv. Mater. Res.*, 2010, **89-91**, p 639-644
- T.S. Price, P.H. Shipway, D.G. McCartney, E. Calla, and D. Zhang, A Method for Characterizing the Degree of Inter-Particle Bond Formation in Cold Sprayed Coatings, *J. Therm. Spray Technol.*, 2007, **16**(4), p 566-570
- G. Bae, S. Kumar, S. Yoon, K. Kang, H. Na, H.-J. Kim, and C. Lee, Bonding Features and Associated Mechanisms in Kinetic Sprayed Titanium Coatings, *Acta Mater.*, 2009, **57**(19), p 5654-5666
- H. Koivuluoto, M. Honkanen, and P. Vuoristo, Cold-Sprayed Copper and Tantalum Coatings—Detailed FESEM and TEM Analysis, *Surf. Coat. Technol.*, 2010, **204**(15), p 2353-2361
- J. Vlcek, L. Gimeno, H. Huber, and E. Lugscheider, A Systematic Approach to Material Eligibility for the Cold-Spray Process, *J. Therm. Spray Technol.*, 2005, **14**(1), p 125-133
- G. Bae, Y. Xiong, S. Kumar, K. Kang, and C. Lee, General Aspects of Interface Bonding in Kinetic Sprayed Coatings, *Acta Mater.*, 2008, **56**(17), p 4858-4868
- R. Kapoor and S. Nemat-Nasser, Determination of Temperature Rise During High Strain Rate Deformation, *Mech. Mater.*, 1998, **27**(1), p 1-12
- J.W. Wu, H.Y. Fang, S. Yoon, H. Kim, and C. Lee, The Rebound Phenomenon in Kinetic Spraying Deposition, *Scr. Mater.*, 2006, **54**(4), p 665-669
- T. Hussain, D.G. McCartney, P.H. Shipway, and D. Zhang, Bonding Mechanisms in Cold Spraying: The Contributions of Metallurgical and Mechanical Components, *J. Therm. Spray Technol.*, 2009, **18**(3), p 364-379
- P. Waldner, Modelling of Oxygen Solubility in Titanium, *Scr. Mater.*, 1999, **40**(8), p 969-974
- H.R.S. Jazi, T.W. Coyle, and J. Mostaghimi, Understanding Grain Growth and Pore Elimination in Vacuum-Plasma-Sprayed Titanium Alloy, *Metall. Mater. Trans. A*, 2007, **38A**(3), p 476-484
- D. Chidambaram, C.R. Clayton, and M.R. Dorfman, Evaluation of the Electrochemical Behavior of HVOF-Sprayed Alloy Coatings-II, *Surf. Coat. Technol.*, 2005, **192**(2-3), p 278-283
- G. Bolelli, L. Lusvardi, and M. Barletta, Heat Treatment Effects on the Corrosion Resistance of Some HVOF-Sprayed Metal Alloy Coatings, *Surf. Coat. Technol.*, 2008, **202**(19), p 4839-4847
- P. Siitonen, S.L. Chen, K. Niemi, and P. Vuoristo, Electrochemical Method for Evaluating the Corrosion Resistance and Porosity of Thermal Sprayed Coatings, *Thermal Spray: International Advances in Coatings Technology*, C.C. Berndt, Ed., May 25-June 5, 1992 (Orlando, FL), ASM International, 1992, p 853-858
- R. Hofman, M.P.W. Vreijling, G.M. Ferrari, and J.H.W. De Wit, Electrochemical Methods for Characterisation of Thermal Spray Corrosion Resistant Stainless Steel Coatings, *Electrochemical Methods in Corrosion Research VI, Pts 1 and 2*, P.L. Bonora and F. Deflorian, Ed., Transtec Publications Ltd, 1998, p 641-653
- N. Ahmed, M.S. Bakare, D.G. McCartney, and K.T. Voisey, The Effects of Microstructural Features on the Performance Gap in Corrosion Resistance between Bulk and HVOF Sprayed Inconel 625, *Surf. Coat. Technol.*, 2010, **204**(14), p 2294-2301
- J.D. Ayers, R.J. Schaefer, F.D. Bogar, and E. McCafferty, Corrosion Behavior of Laser Consolidated Titanium Coated Steel in Sea-Water, *Corrosion*, 1981, **37**(1), p 55-57
- J. Kawakita, S. Kuroda, T. Fukushima, and T. Kodama, Development of Dense Corrosion Resistant Coatings by an Improved HVOF Spraying Process, *Sci. Technol. Adv. Mater.*, 2003, **4**(4), p 281-289
- R.C. McCune, W.T. Donlon, O.O. Popoola, and E.L. Cartwright, Characterization of Copper Layers Produced by Cold Gas-Dynamic Spraying, *J. Therm. Spray Technol.*, 2000, **9**(1), p 73-82
- T. Valente and F.P. Galliano, Corrosion Resistance Properties of Reactive Plasma-Sprayed Titanium Composite Coatings, *Surf. Coat. Technol.*, 2000, **127**(1), p 86-92